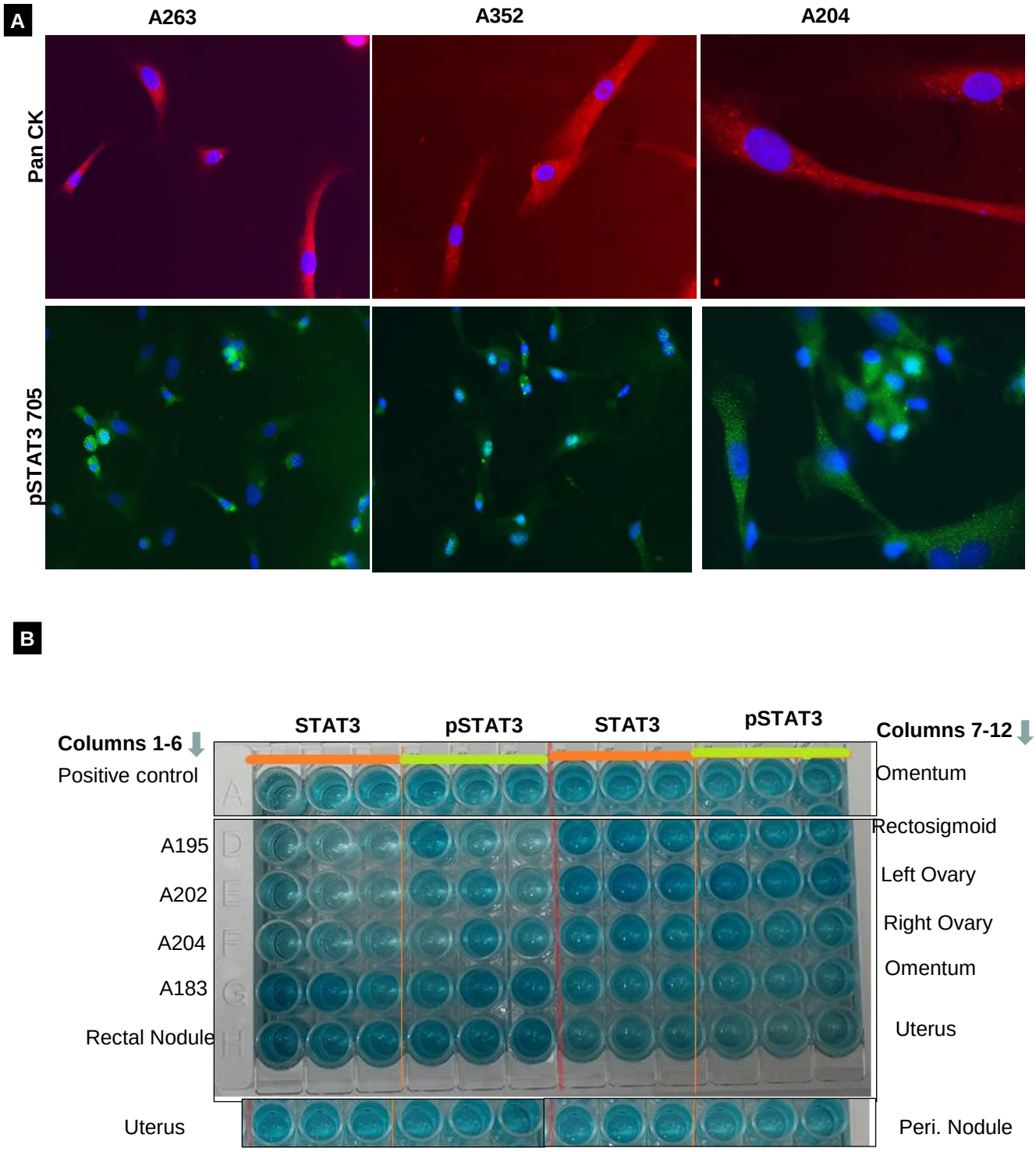

Fig. S1A: Characterization of ascites derived ovarian cancer cells (ADOCCs – A183 to A352) from additional patients. Pan CK is the epithelial origin specific marker (top panel) and pSTAT3705 demonstrates pSTAT3 705 expression.
S1B: ELISA plate displaying total STAT3 and pSTAT3 expression in ADOCCs, primary ovary tumor and metastasized sites from consented patients

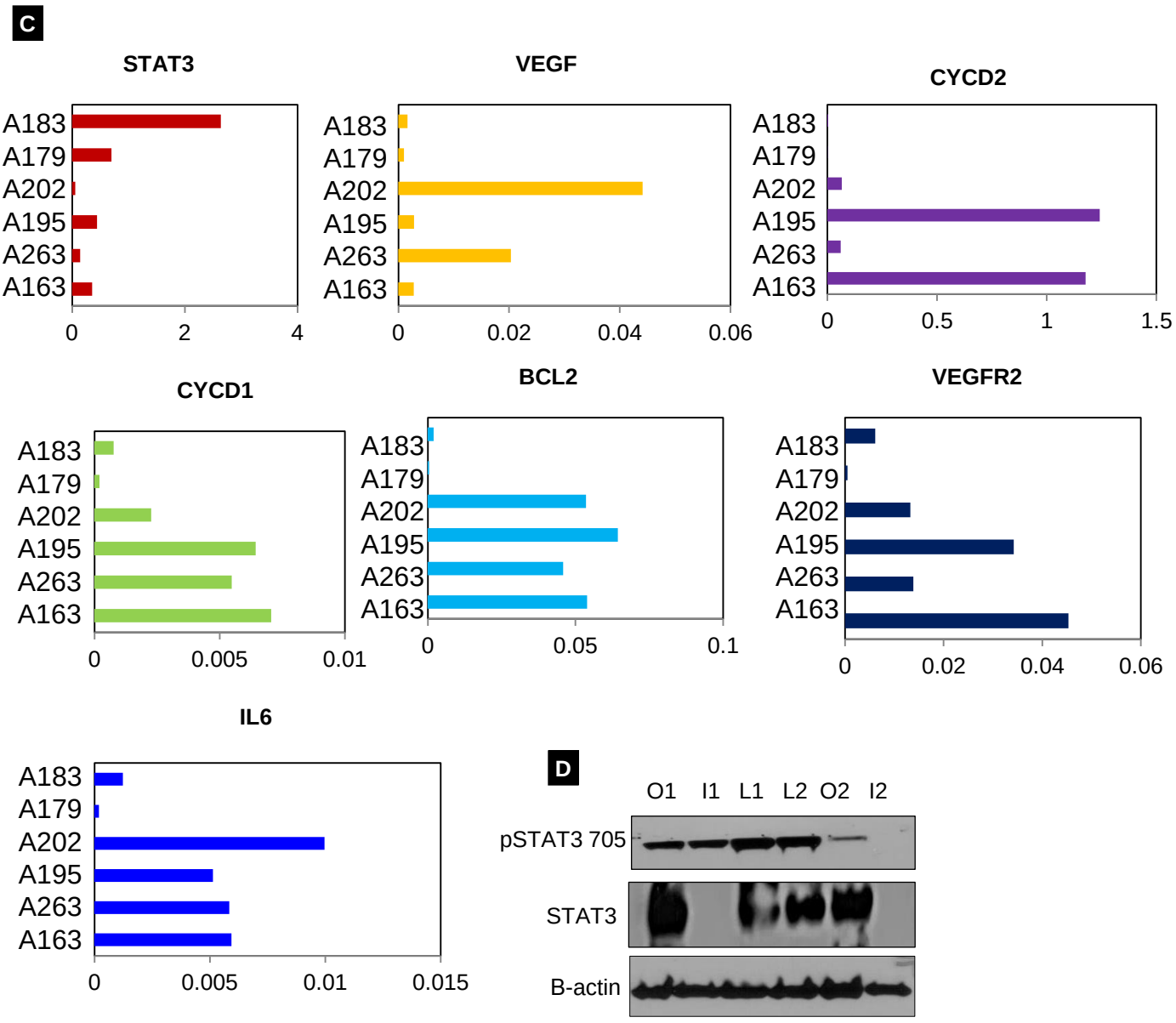

Fig. S1C: Real Time quantitative PCR results for relative RNA expression for ADOCCs displaying STAT3 and other regulatory genes like VEGF, CYC D2, CYC D1, BCL2, VEGFR2 and IL6. The expression for each was normalised to GAPDH. (**D**) Panel H shows the protein expression using Western blot of the organs collected from the tumor mice [STAT3 OE mice (O1, I1 and L1) and A2780 Wt mice (L2, O2 and I2) at the time of sacrifice (O-ovary, I-intestine and L-liver).

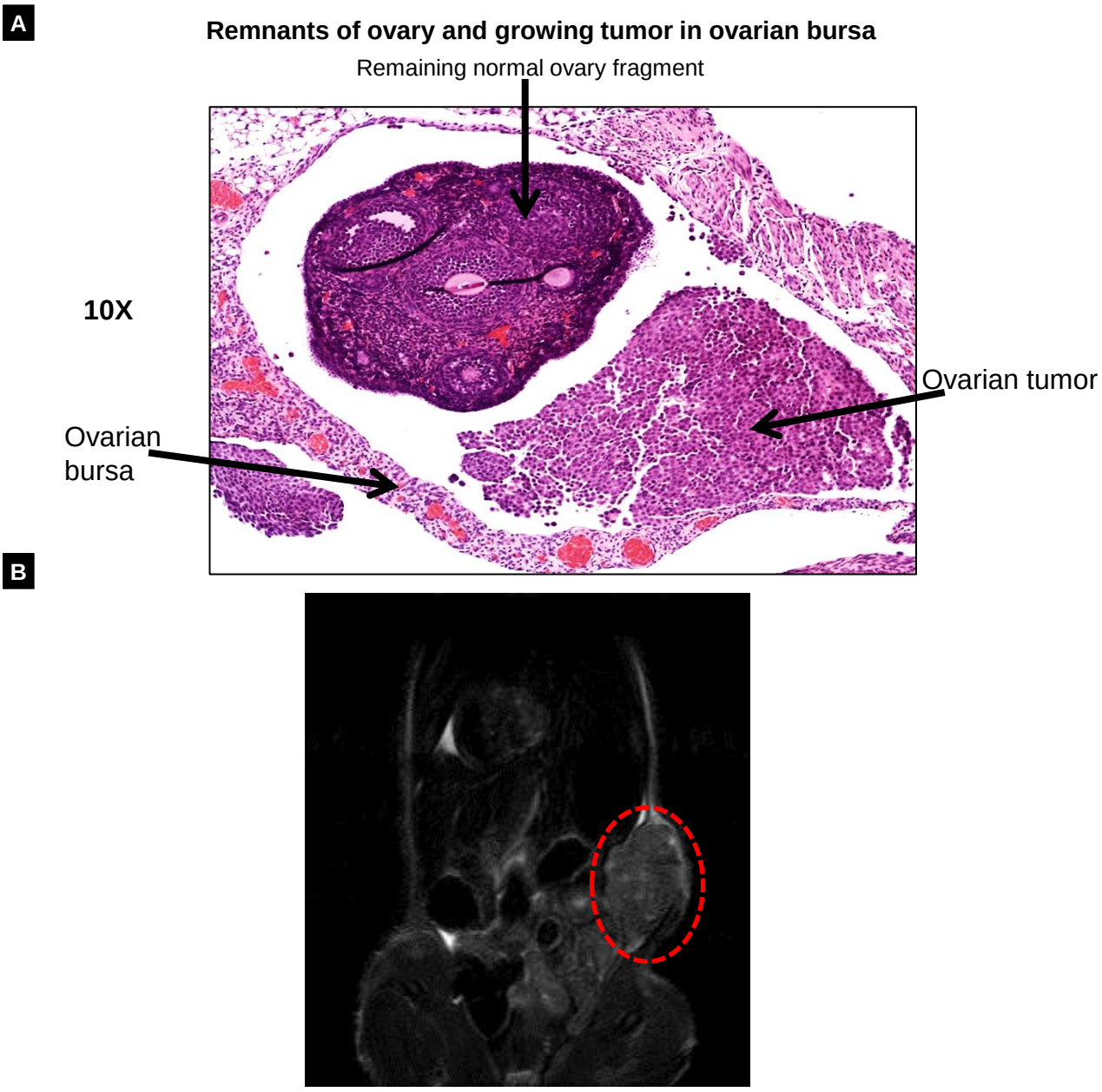

Fig. S2: (**A**) Human ovarian cancer cells (A2780) (100000 cells in 5µl of PBS) were injected into right ovarian bursal cavity in nude mice.
(**B**) MRI image showing ovarian tumor growth.

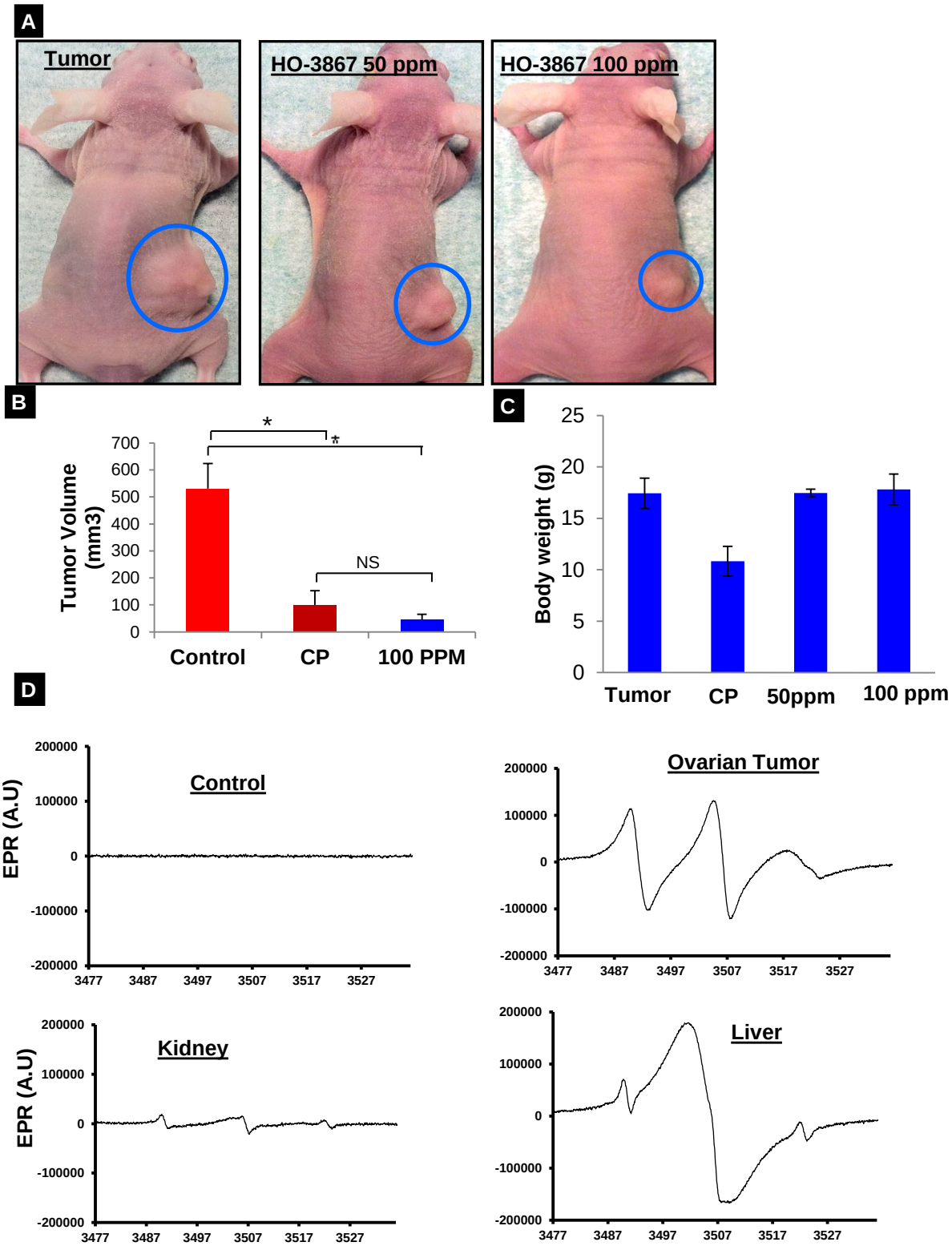

Fig. S3: (**A**) Additional mice showing the efficacy of HO-3867 on mice tumors (**B**) Tumor volume, HO-3867–treated animals were significantly reduced the tumor volume (**C**) body weight in each group upon completion of the treatment period (**D**). HO-3867 levels in the ovarian tumor, kidney and liver tissue samples were determined using EPR.

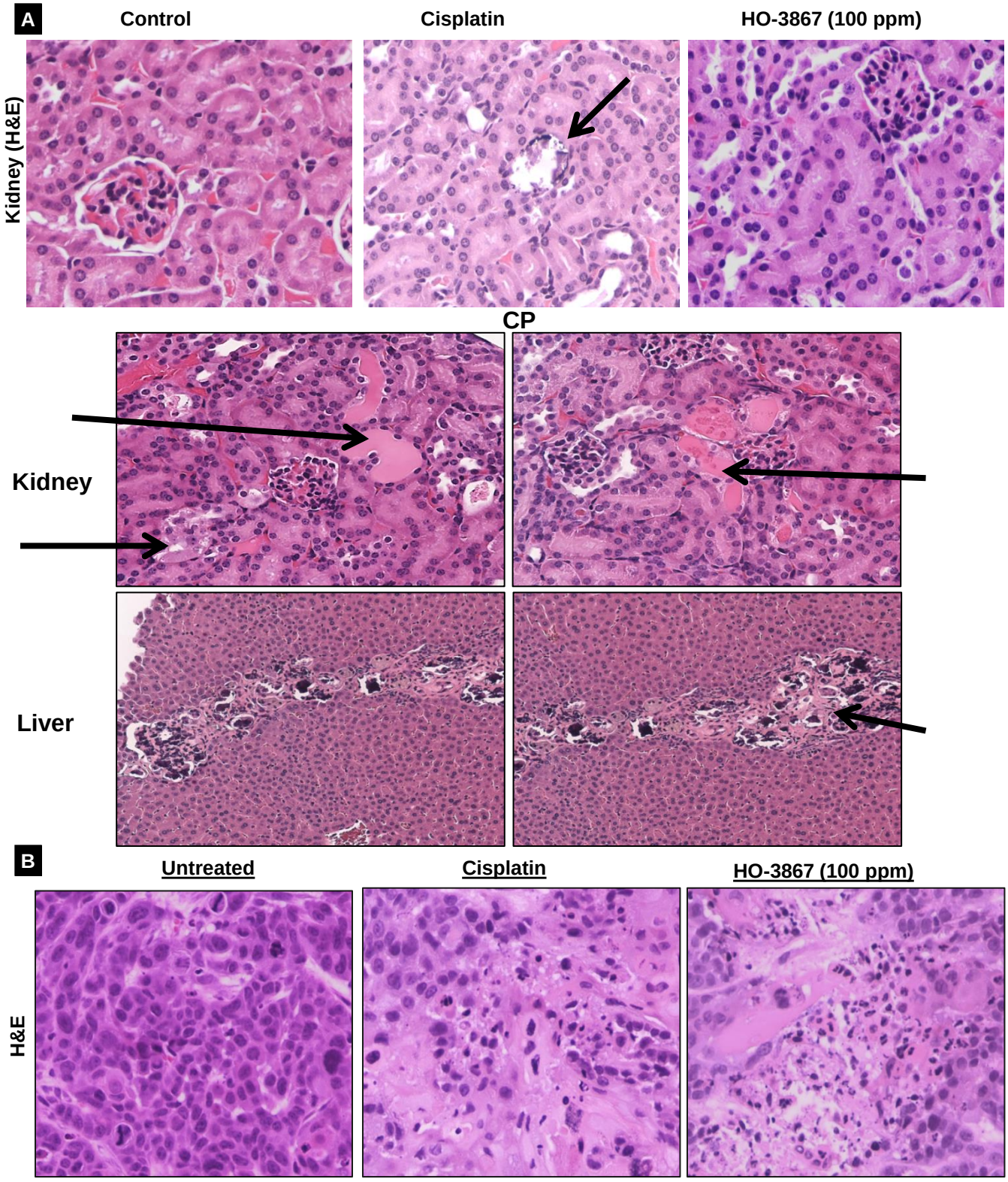

Fig. S4: nephrotoxicity staining in kidney : (**A**) cisplatin-treated animal consistently showed evident nephrotoxicity characterized by areas of loss and necrosis of tubular epithelial cells which were calcified (arrow), and protein cast in the tubular lumen (arrowhead) consistent with proteinuria (kidney and liver images from 3 different mice). Further cisplatin-treated animals showed hepatotoxicity with linear areas of necrosis of periportal hepatocytes, accompanied by fibrosis and calcification (arrow). Liver images for 2 different mice (**B**) In addition, the H&E staining showed that the HO-3867 selectively induces necrosis in tumor.

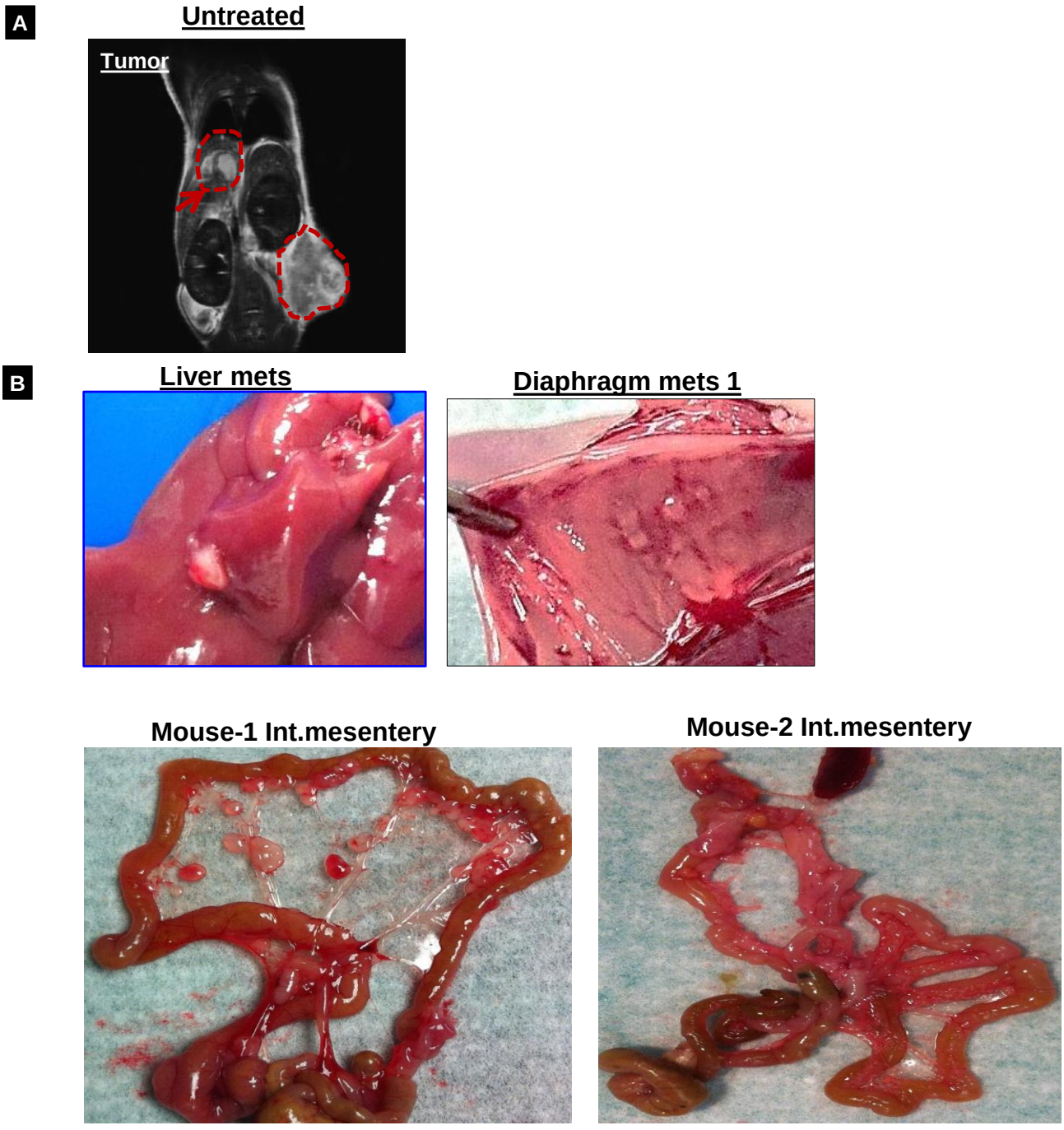

Fig. S5: (**A**) MRI image of tumor metastasized to liver in the orthotopic mouse model (**B**) Additional pictures displaying metastasis to liver, diaphragm and internal mesentery

C

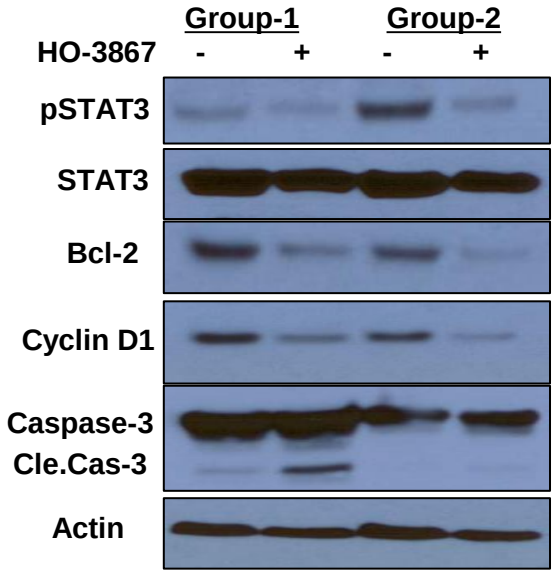

Fig. S5: Western blot showing the variations in expression of STAT3 and related genes from two different mice group tumor tissues which were either untreated control (-) or HO-3867 treated (+) for each group

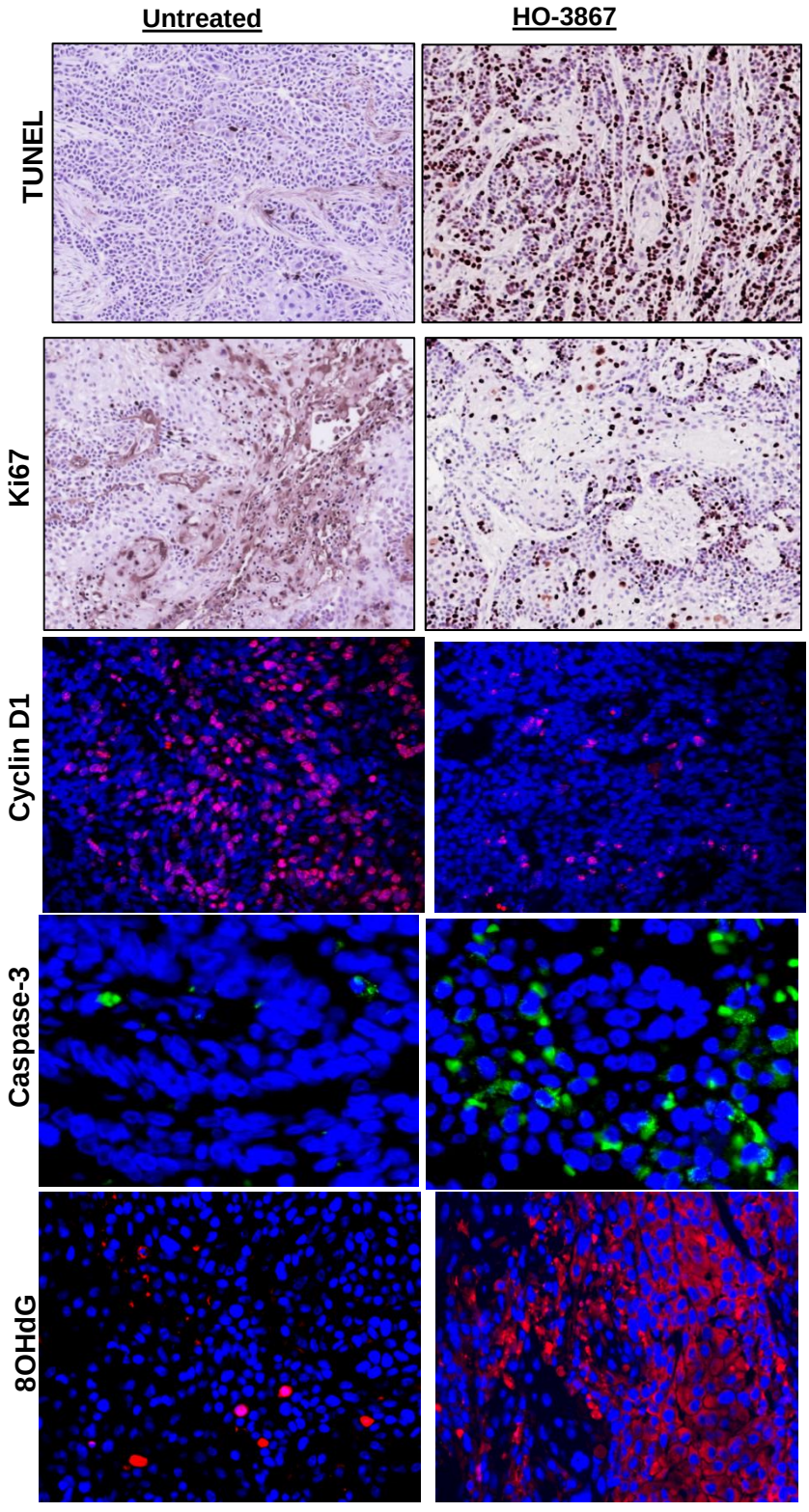

Fig. S6: HC analysis confirmed the increased cleaved caspase-3 and decreased Cyclin-D levels in HO-3867 treated tumors

A

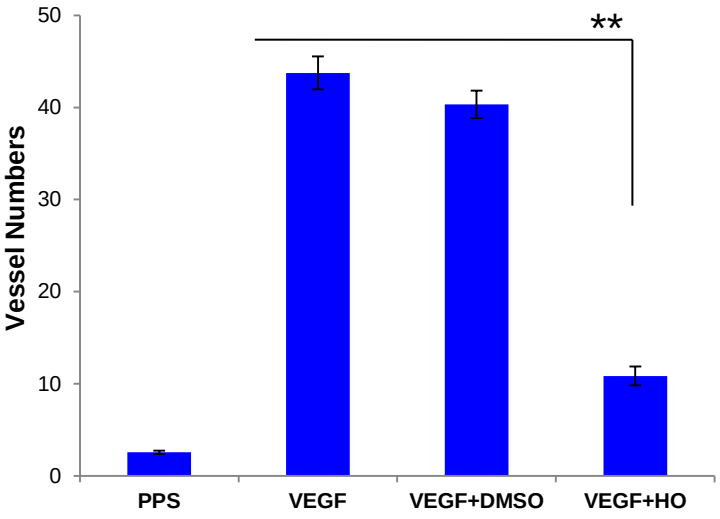

B

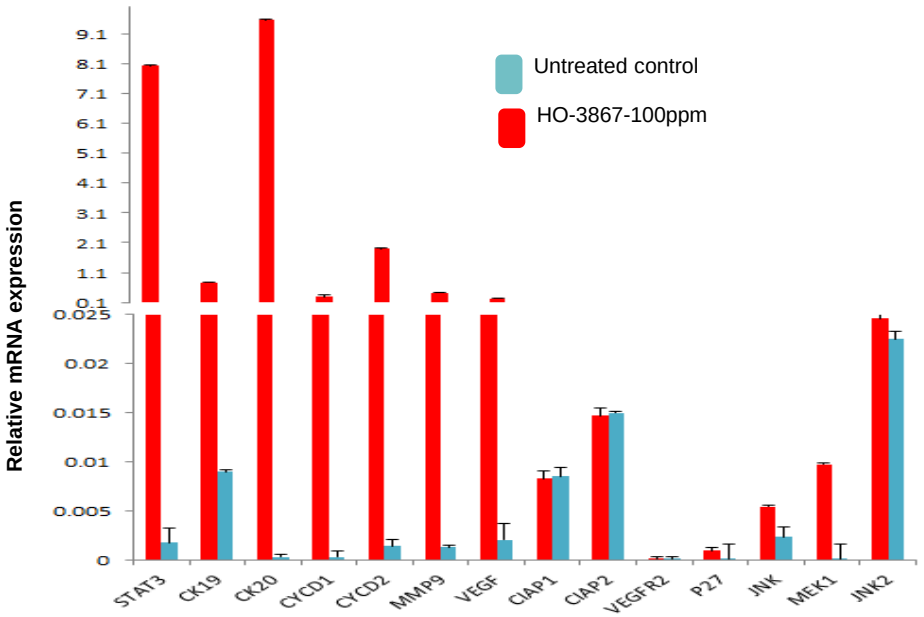

(**A**) In vivo Matrigel assay, sections were stained for CD34 staining. The numbers of CD34 positive vessels per high power field were counted for each experimental condition ($p<0.005 n=3$).
(**B**)Relative gene expression of STAT3 and its regulatory genes in response to HO-3867 treatment in mouse ovarian tumor tissue.

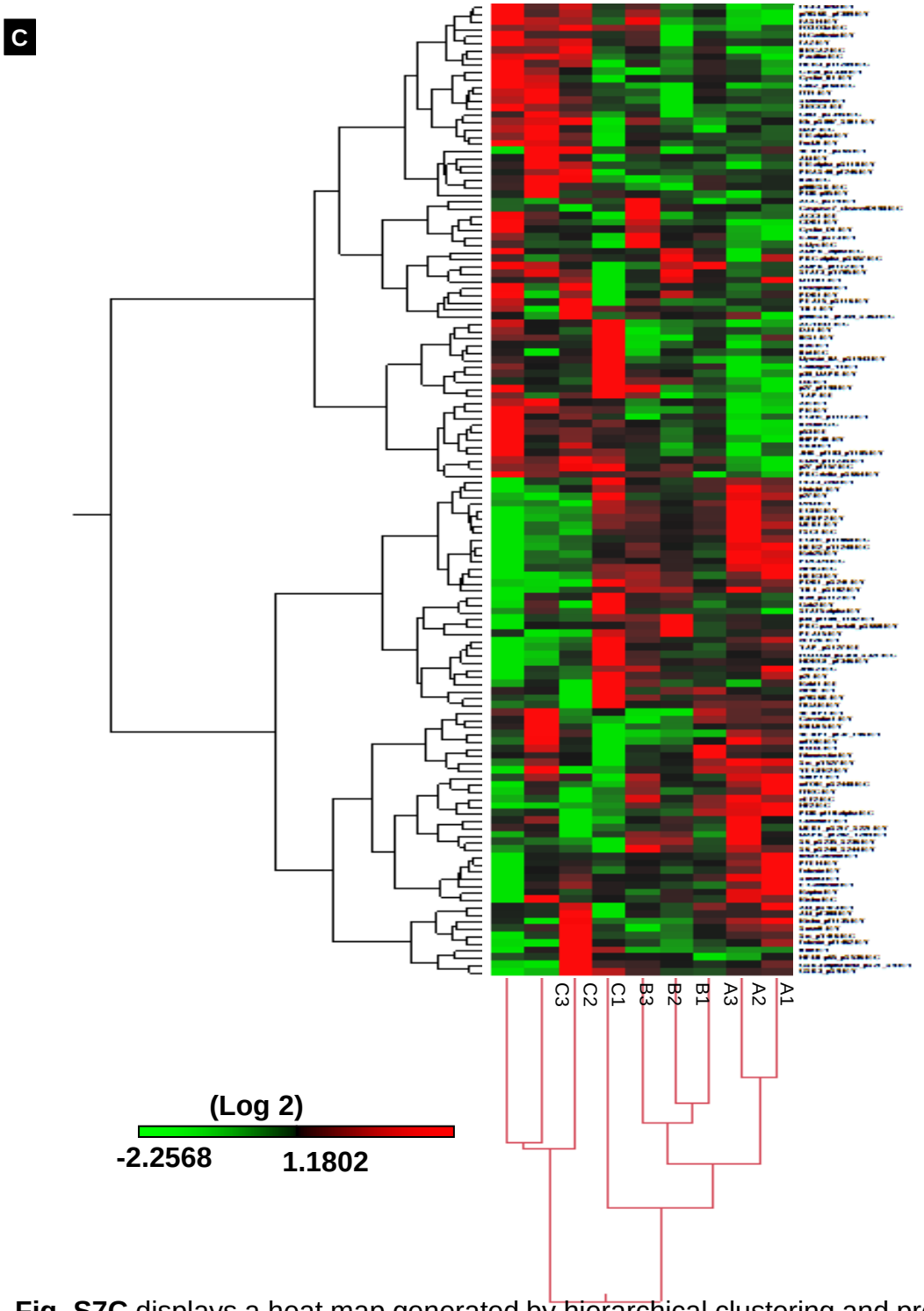

Fig. S7C displays a heat map generated by hierarchical clustering and presenting a grid of colored points for the untreated tumor samples (vertical axis, lanes 1-3) and HO-3867 treated samples. Clustered heat maps illustrate differential protein expression profiles across 9 samples of three experiment conditions- A, B, and C with each condition applied to 3 biological repeat samples. Each color represents a protein expression value. The proteins of interest are shown on the horizontal axis. Red corresponds to high expression, black intermediate, and green low expression relative to a common reference standard.

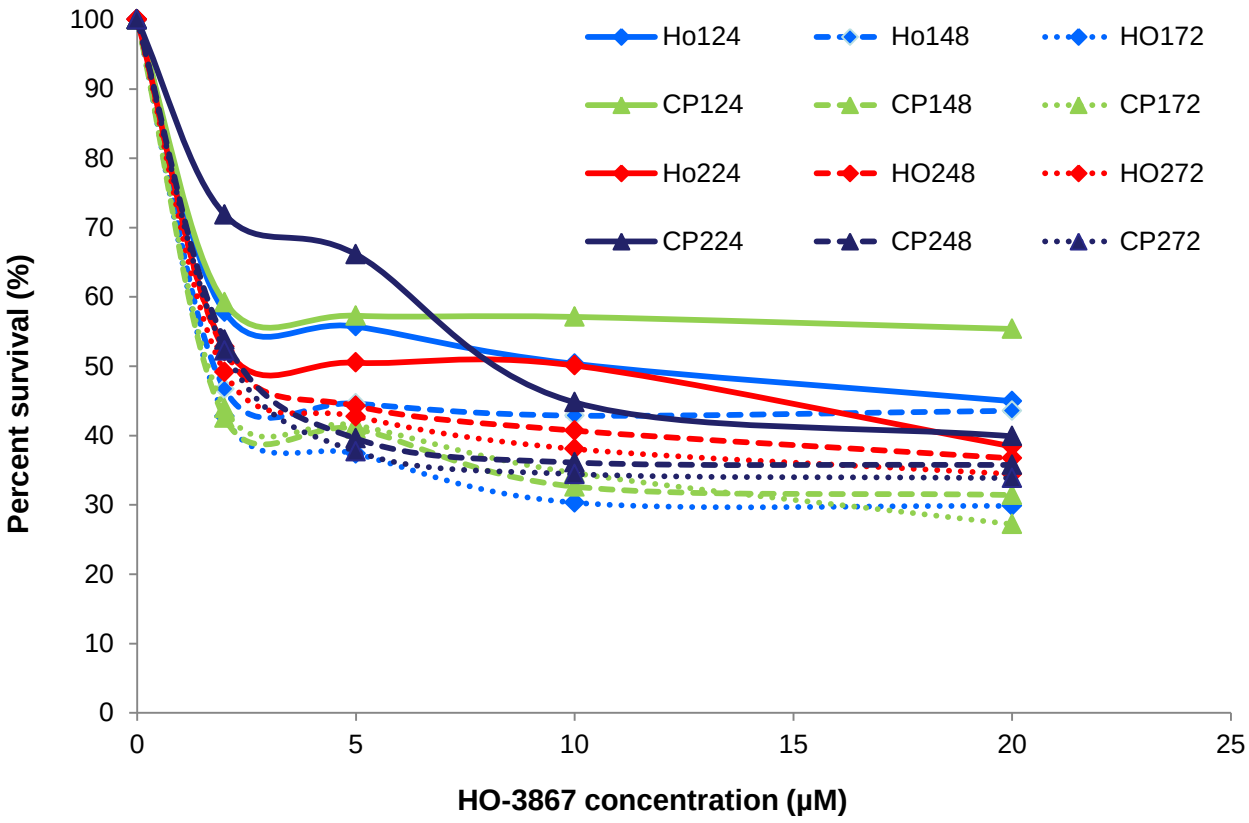

Fig. S8: Sulforhodamine B assays for percent cell proliferation of 2 different human ascites derived cancer cells (1: A 352 and 2: A204) after treatment with HO-3867 and Cisplatin for various time points and different concentrations.

Fresh human ovarian tumors (HGSC) transported from surgery room in ice.

Tumors are embedded on a 1% agarose gel block using superglue, and mounted on vibratome

400 um-thick tissue slices were made and transferred into 6-well plates containing culture medium

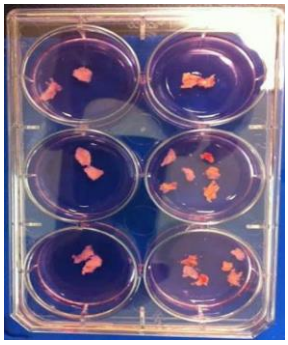

At specific time points, tissue slices were removed from culture plates.
- Fixed in formalin for 24-48 hours

Traditional histology processing
Paraffin embedded & 4 um tissue sections were made on glass slide

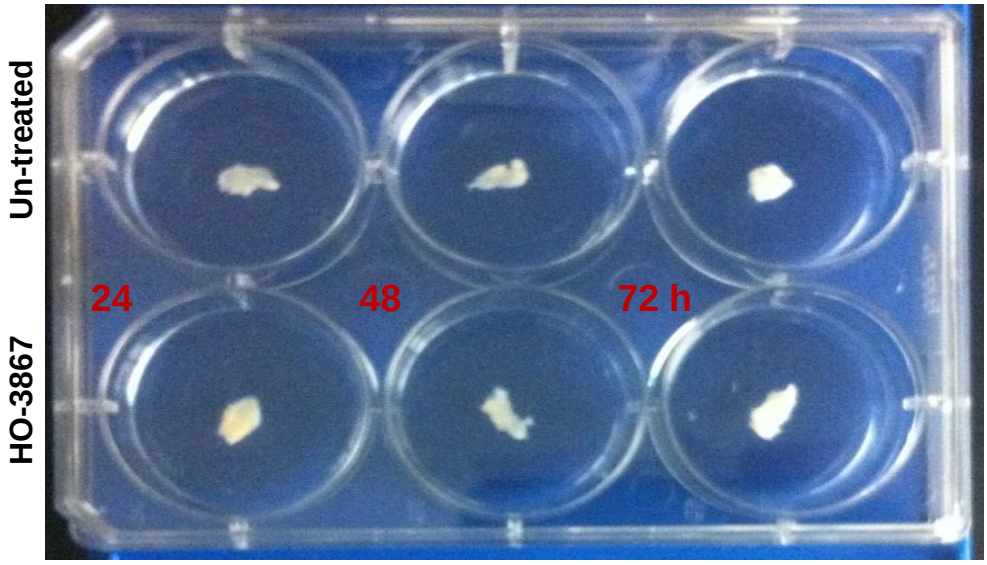

Fig. S9: Schematic displaying the process of slicing the freshly collectd human ovarian cancer tissue sections which are embedded in an agarose gel and sliced into 400Um slices using a vibratome. The slices were treated with HO-3867 and samples were fixed in formalin at 24 and 48 hours' time points followed by paraffin embedding and sectioning into 4Um sections.

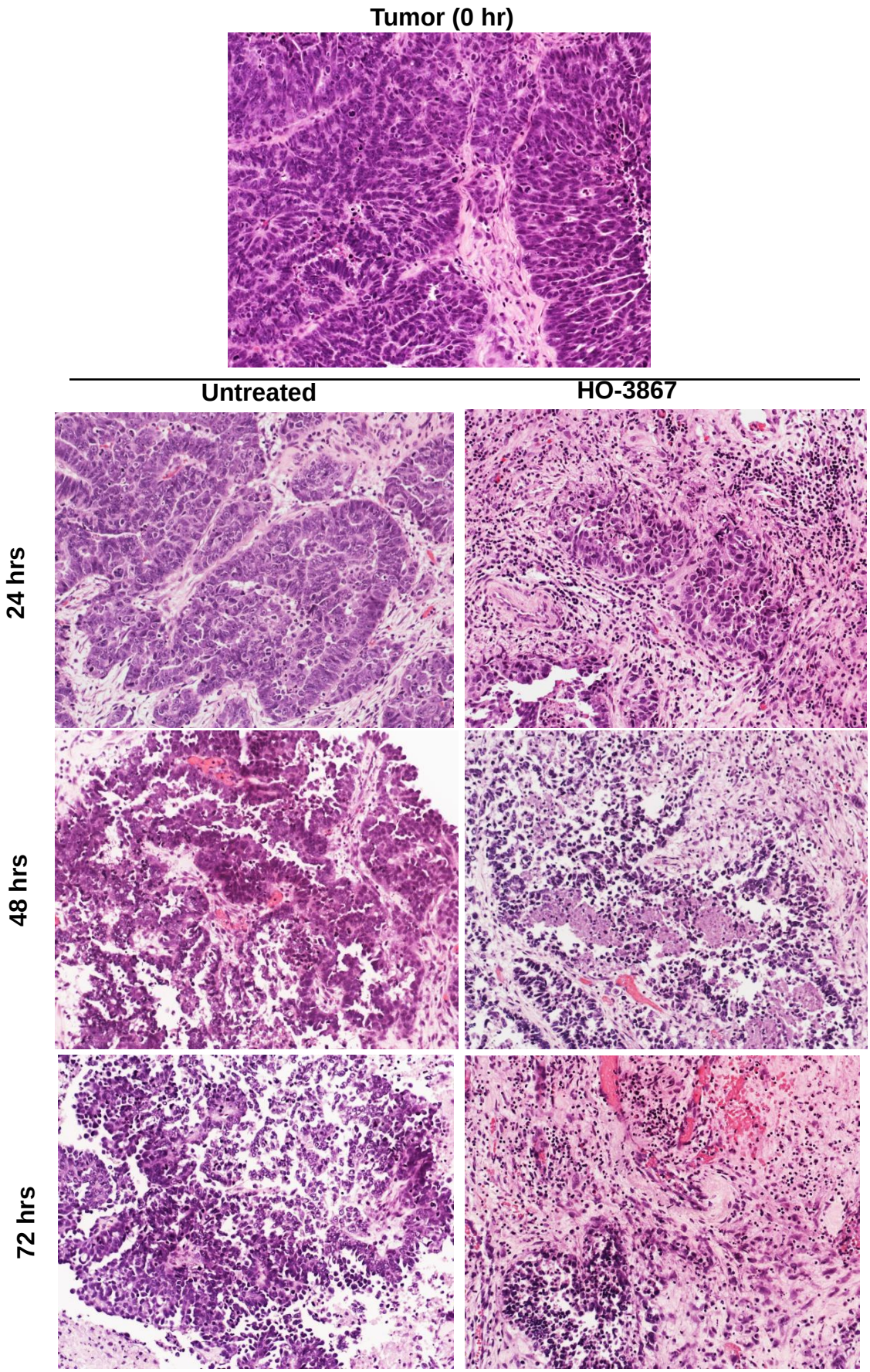

Fig. S9: IHC of additional human ovarian tumor samples with or without treatment with HO-3867 at different time points.

72 hrs Treatment with HO-3867, CP and STATTIC in 4 different patient tumor tissues

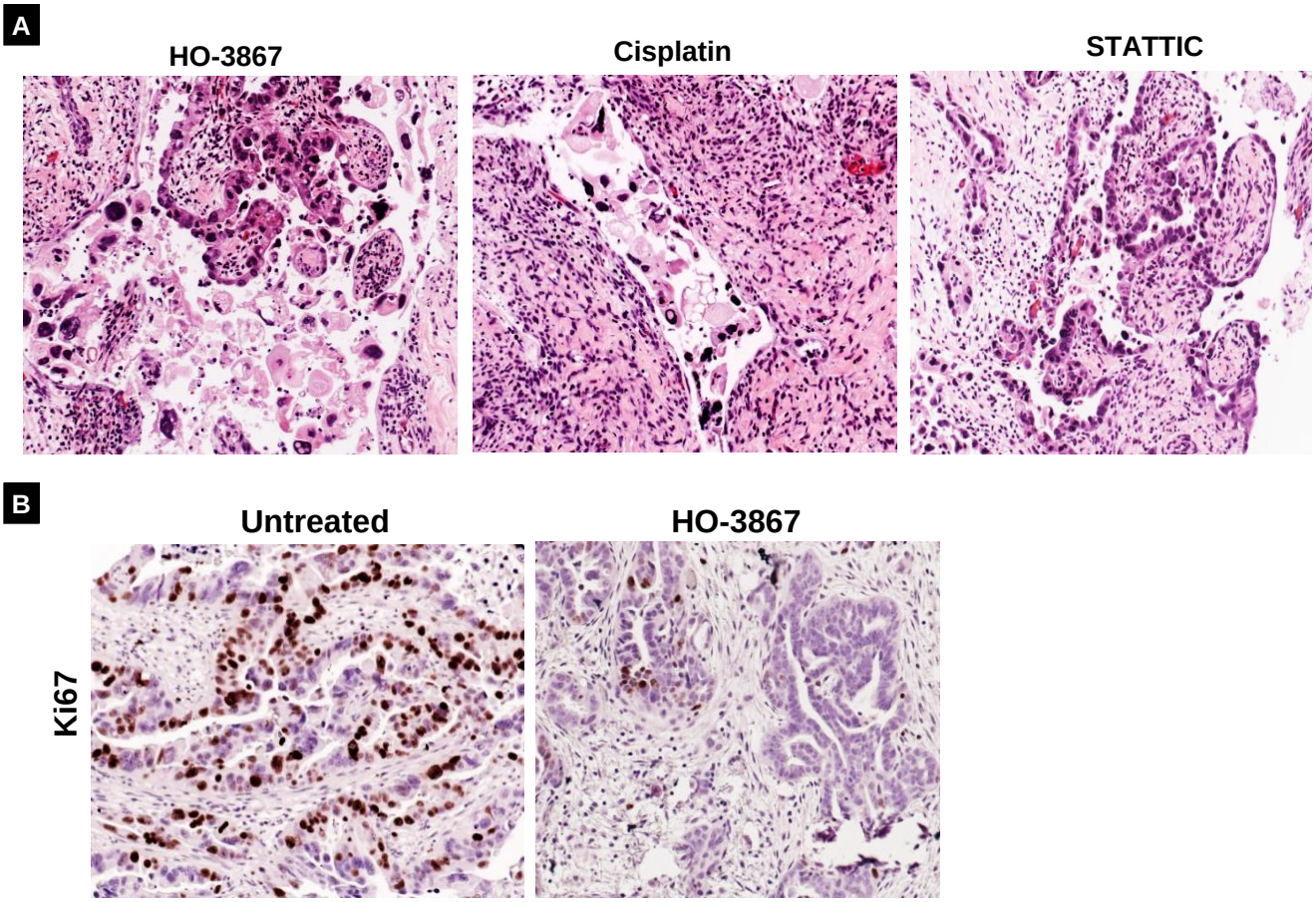

Fig. S11: IHC of additional ovarian tumor samples with or without treatment with HO-3867, Cisplatin or Static at 72 h (Panel A). Ki67 staining in untreated and HO-3867 treated human ovarian tumor sample (Panel B).

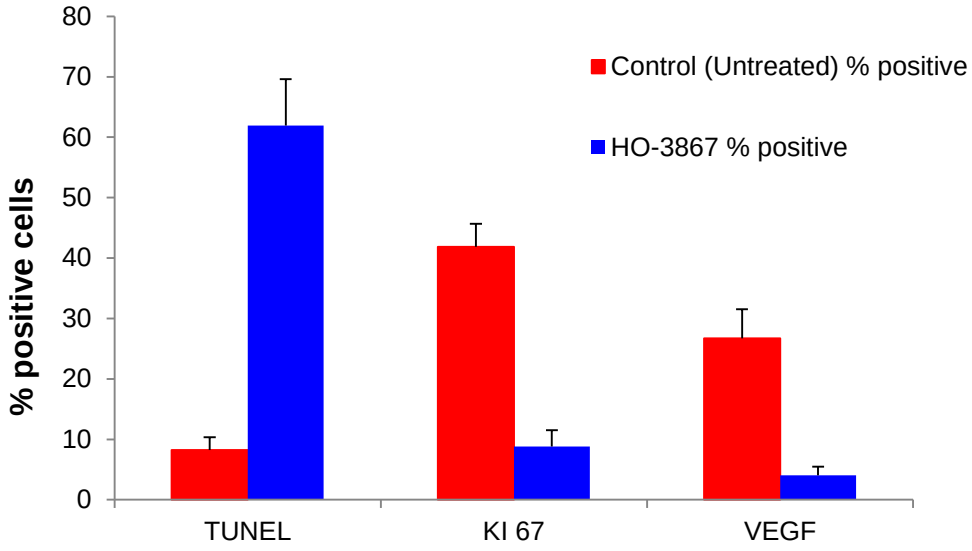

Fig. S12: Quantification for TUNEL, Ki67, and VEGF from ex vivo samples untreated Vs HO-3867 treated. The graph represents mean from 3 different slides of the same sample and counted for total cells, positive and negative cells to calculate a percent value.

Sup. Table 1.
H3867 cellular uptake and its M+4 metabolite concentrations found in primary ovarian cancer cell (POCC) population samples after treatment with 10µM H3867

Label	Cell Type	Treatment	H3867 (ng/mL/10^6 cells)	H3867 M+4 * (ng/mL/10^6 cells)
C	POCC	none		
0	POCC	10µM H3867	1.48 ± 0.37	381.6 ± 61.0
1	POCC	10µM H3867	13.62 ± 3.18	643.8 ± 129.0
3	POCC	10µM H3867	12.69 ± 1.90	2439.7 ± 152.7
6	POCC	10µM H3867	1.5 ± 0.30	571.4 ± 95.6

Table 1. H3867 cellular uptake and metabolite quantification**.** OVCAR8 and TR127 were also treated with 10µM H3867 at 0, 1, 3 and 6 hours. During sample analysis, the M+4 reduced metabolite identified from intracellular profiling was also included in the assay and simultaneously monitored by ion transitions m/z 469.20>436.20 along with H3867 m/z 465.2> 432.2. With absence of authentic chemical standard, the M+4 metabolite concentration was quantified against the calibration standard curve of H3867 in cells. As shown in Table 1, the intracellular H3867 concentrations were relatively low as compared to H3867 M+4 metabolite level. Therefore, H3867 was quickly and extensively metabolized within cell to convert to metabolite M+4.